Conductivity and structure of ErAs nanoparticles embedded in GaAs pn junctions analyzed via conductive atomic force microscopy

K. W. Park, V. D. Dasika, H. P. Nair, A. M. Crook, S. R. Bank et al.

Citation: Appl. Phys. Lett. **100**, 233117 (2012); doi: 10.1063/1.4728116
View online: http://dx.doi.org/10.1063/1.4728116
View Table of Contents: http://apl.aip.org/resource/1/APPLAB/v100/i23
Published by the American Institute of Physics.

Conductivity and structure of ErAs nanoparticles embedded in GaAs pn junctions analyzed via conductive atomic force microscopy

K. W. Park, V. D. Dasika, H. P. Nair, A. M. Crook, S. R. Bank, and E. T. Yu[a)]
Microelectronics Research Center, University of Texas at Austin, 10100 Burnet Rd., Austin, Texas 78758, USA

(Received 27 January 2012; accepted 23 May 2012; published online 6 June 2012)

We have used conductive atomic force microscopy to investigate the influence of growth temperature on local current flow in GaAs pn junctions with embedded ErAs nanoparticles grown by molecular beam epitaxy. Three sets of samples, one with 1 ML ErAs deposited at different growth temperatures and two grown at 530 °C and 575 °C with varying ErAs depositions, were characterized. Statistical analysis of local current images suggests that the structures grown at 575 °C have about 3 times thicker ErAs nanoparticles than structures grown at 530 °C, resulting in degradation of conductivity due to reduced ErAs coverage. These findings explain previous studies of macroscopic tunnel junctions. © *2012 American Institute of Physics*. [http://dx.doi.org/10.1063/1.4728116]

The incorporation of rare earth-V (RE-V) semimetallic nanoparticles in III-V compound semiconductors can provide substantial performance enhancements in device applications such as tunnel junctions in tandem solar cells, thermoelectric devices, and ultrafast optical switches.[1–3] For the most extensively explored RE-V/III-V combination, ErAs/GaAs, previous work has established that rock-salt, semimetallic ErAs nanoparticles can self-assemble on a GaAs surface in an islanding growth mode[4] with subsequent overgrowth by high-quality GaAs.[5] Although there are many applications in which ErAs nanoparticles have yielded improvement in device performance, further optimization of device characteristics requires an improved understanding of electrical properties of ErAs nanoparticles and their dependence on growth conditions. For example, a previous study[6] observed increased resistivity of ErAs/GaAs tunnel junction grown at elevated temperatures in macroscopic device measurements; however, the detailed structure and nature of current flow are not well understood.

In this Letter, we employed conductive atomic force microscopy (C-AFM) to explore the nanoscale tunneling current enhancement enabled by ErAs nanoparticles embedded in GaAs and to elucidate the structural and electrical properties of ErAs nanoparticles under different growth conditions. Since C-AFM is able to characterize electronic behavior in III-V semiconductors at the nanoscale,[7,8] we have probed the nature and spatial distribution of tunnel junction conductivity to elucidate the origin of reduced conductivity in tunnel junctions grown at elevated temperatures.

A schematic of the sample structure and the C-AFM measurement setup is shown in Fig. 1(a). A silicon probe tip coated by boron-doped diamond, which was kept at a constant deflection to maintain the same contact force to the sample surface, was connected directly to an external current preamplifier (ITHACO 1211). The amplified current signal was then sent to the AFM controller and software. All current measurements in this paper were conducted at room temperature and ambient environment using a +0.5 V dc bias applied to the sample stage, and collected signals were amplified by 10^7 V/A transimpedance amplifier. The deflection set point was minimized to prevent excessive wearing of the conductive coating on the probe during scanning.

The samples were grown in a Varian Gen II solid-source molecular beam epitaxy (MBE) system. The sample structures consisted of ErAs nanoparticles embedded at the p-n interface of a GaAs pn junction and were grown on n-GaAs (001) substrates. Following the deposition of 200 nm n^+

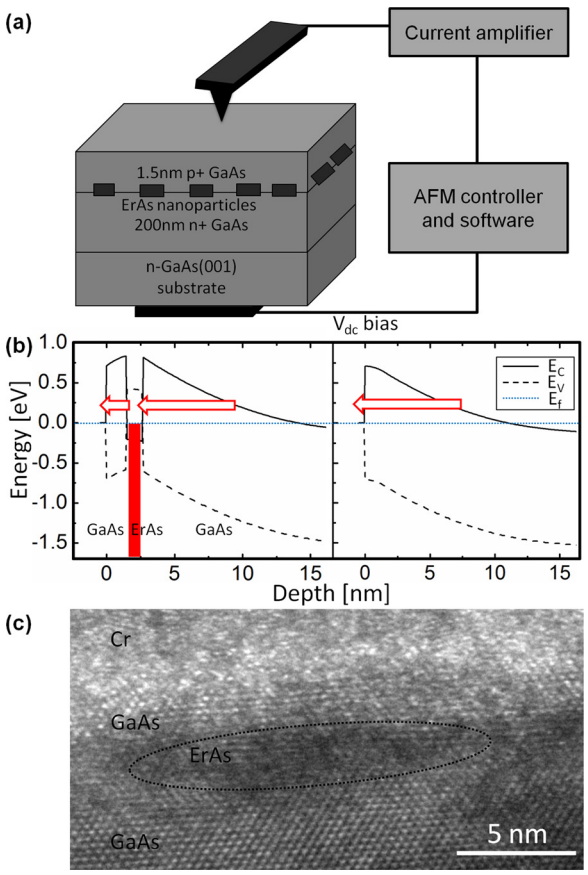

FIG. 1. (a) Schematic diagram of GaAs/ErAs pn junction sample, conductive AFM measurement geometry, and electrical connections. (b) Energy band-edge diagram for GaAs pn junction with embedded ErAs nanoparticle (left) and GaAs-only pn junction (right). (c) Cross-sectional TEM images for the sample grown at 575 °C with 1.6 ML of ErAs deposition.

[a)]Electronic mail: ety@ece.utexas.edu.

GaAs (Si doped, $\sim 5 \times 10^{18}\,\mathrm{cm}^{-3}$), ErAs was deposited to form nanoparticles, and capped with 1.5 nm of p^+ GaAs (Be doped, $\sim 5 \times 10^{19}\,\mathrm{cm}^{-3}$). Growth temperature ranged from 485 °C to 575 °C, and the ErAs deposition levels ranged from 0.4 ML to 1.6 ML.

Figure 1(b) shows energy band-edge diagrams for a GaAs/ErAs pn junction and a GaAs-only pn junction, obtained by numerical solution of Poisson's equation in one dimension. As indicated schematically, electrical current flow is enhanced in the former structure via a two-step tunneling process enabled by the ErAs nanoparticles.[1,6] This is expected to occur for either structures with thin, depleted cap layer, as shown in Fig. 1(b), or for complete pn tunnel junctions. Cross-sectional transmission electron microscopy (TEM) images were obtained to confirm that the 1.5 nm p^+ GaAs capping layer was sufficient to cover the ErAs nanoparticles and prevent their oxidation. A TEM image for the sample grown at 575 °C with 1.6 ML ErAs is shown in Fig. 1(c), as wetting of ErAs by GaAs decreases with increasing growth temperature and this sample therefore represents that for which incomplete ErAs nanoparticle coverage by the GaAs capping layer is expected to be most problematic. As is evident from the figure, the ErAs nanoparticle is completely overgrown by GaAs and oxidation of the ErAs is not observed. The Cr layer visible in the image was deposited on the GaAs surface as part of a standard TEM sample preparation process.

To further assess the potential impact of oxidation of ErAs nanoparticles capped with only a thin 1.5 nm p^+ GaAs layer, we also performed C-AFM measurements on samples with an ErAs nanoparticle layer and GaAs capping layers up to 30 nm in thickness, and on control samples with a 1.5 nm GaAs capping layer with no ErAs. Samples with a 1.5 nm GaAs capping layer and an ErAs nanoparticle layer showed much greater current flow than otherwise identical GaAs pn junctions with no ErAs deposition, consistent with the presence of unoxidized ErAs nanoparticles. In addition, conductivity measurements did not degrade in repeated measurement over time, which also suggests that oxidation has little if any effect on electrical conductivity over extended time periods.

Previous TEM studies revealed varying ErAs nanoparticle morphology and size for different ErAs deposition amount and growth temperature,[9,10] so variation in the electrical properties with growth conditions is expected. Therefore, we prepared an initial set of samples to assess the dependence of current density on growth temperature. GaAs pn junctions with embedded ErAs nanoparticles were grown at 485 °C, 515 °C, 545 °C, and 575 °C with ErAs deposition fixed at 1 ML. Figure 2(a) shows local current images for these samples with surface topography from the sample grown at 485 °C. Dark regions in the current images indicate locations of high current flow. C-AFM images for the samples grown at 485–545 °C displayed similar current densities, while the sample grown at 575 °C yielded a lower overall current density due to a lower density of conductive locations. Figure 2(b) shows the average current densities derived from multiple measurements for each sample. Decreased current density at high growth temperature is evident. Figure 2 also suggests that the sample grown at 575 °C

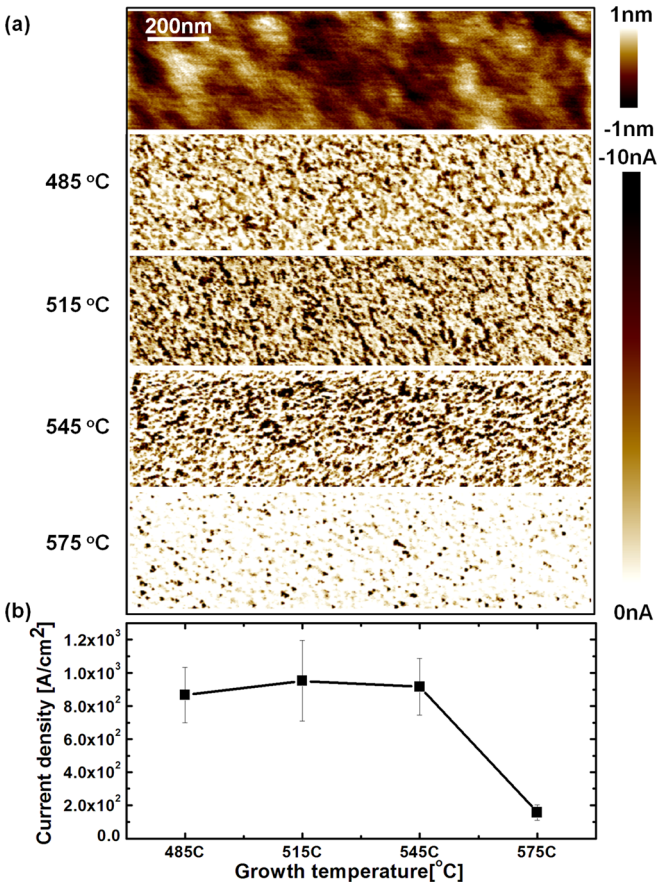

FIG. 2. (a) C-AFM images for samples grown at 485 °C, 515 °C, 545 °C, and 575 °C with 1 ML of ErAs deposition measured with a sample bias 0.5 V, with AFM topography obtained from a sample grown at 485 °C. (b) Current densities derived from C-AFM images for each growth temperature.

has different ErAs morphology, based on the sparse conductivity distribution, as compared with the samples grown at lower temperatures. These observed current densities are consistent with those obtained in macroscopic device measurements.[6]

To further elucidate the influence of growth temperature on ErAs nanoparticle morphology and electrical conductivity, two additional sample sets were studied. These structures were grown at fixed growth temperatures of either 530 °C or 575 °C, with ErAs deposition of 0.4 ML, 0.8 ML, 1.2 ML, or 1.6 ML. Figures 3(a) and 3(b) show current images for varying ErAs depositions at each growth temperature. The average current densities derived from multiple measurements, as functions of both growth temperature and ErAs deposition, are shown in Fig. 3(c). The current density for a growth temperature of 530 °C increases linearly with ErAs deposition, suggesting a linear increase in ErAs nanoparticle interface coverage with a constant ~3–4 ML nanoparticle thickness. In contrast, the samples grown at 575 °C show both lower overall current density and non-linear dependence on the amount of ErAs deposition. The current densities in pn junctions with 0.4 ML and 0.8 ML ErAs were similar to those of the reference sample (a pn junction without ErAs nanoparticles), whereas the samples with 1.2 ML and 1.6 ML ErAs exhibited increased tunneling current. This suggests that the conductivity of samples with 0.4 ML and 0.8 ML ErAs is minimally influenced by the presence of the

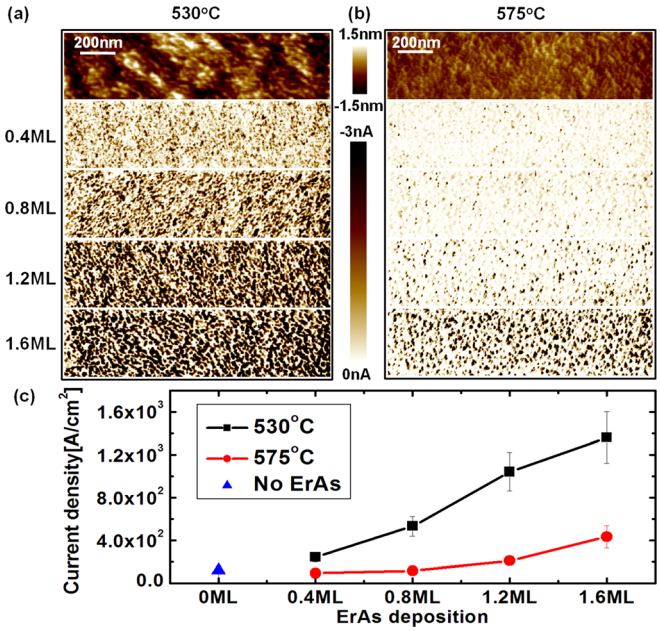

FIG. 3. C-AFM images for samples with 0.4 ML, 0.8 ML, 1.2 ML, and 1.6 ML ErAs grown at (a) 530 °C and (b) 575 °C, with AFM topography obtained from a 1.6 ML ErAs deposition sample. (c) Current densities derived from C-AFM images for different ErAs deposition levels including a reference sample without ErAs, for each growth temperature. Sample bias was 0.5 V for the C-AFM measurement.

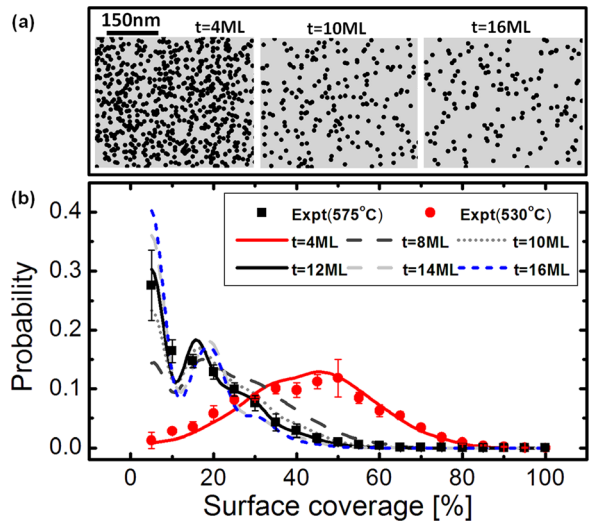

FIG. 4. (a) Representative simulated distributions of ErAs nanoparticles (black circles) for a fixed nanoparticle radius of 6 nm and thicknesses of 4 ML (left), 10 ML (center), and 16 ML (right) for total ErAs deposition of 1.6 ML. (b) Modeled (lines) distribution of local ErAs coverage for GaAs/ErAs samples with 1.6 ML ErAs and ErAs nanoparticle thicknesses of 4 ML-16 ML, along with measured (symbols) local ErAs coverage distribution for samples grown with 1.6 ML ErAs at 530 °C and 575 °C. At 530 °C, the coverage distribution corresponds closely to that expected for an ErAs nanoparticle thickness of 4 ML; while at 575 °C, the coverage distribution matches that for 10–12 ML ErAs nanoparticle thickness.

ErAs nanoparticles, while conductivity for structures with 1.2 ML and 1.6 ML ErAs benefits substantially from the tunneling current enhancement through the ErAs nanoparticles, which increases with ErAs deposition in this range. This unusual dependence can be attributed to the combined effect of increased vertical extent of nanoparticles at high growth temperature and increased nanoparticle coverage at high ErAs deposition levels.[10]

To investigate the vertical extent of ErAs nanoparticles at different growth temperatures, we combined statistical analysis of spatial inhomogeneity of the C-AFM images with simulations of the statistical distribution of ErAs nanoparticle coverage for different ErAs nanoparticle thicknesses. For this analysis,[11] we defined a threshold C-AFM signal level such that the fraction of points in the image below this threshold level (i.e., more conductive) corresponded to the fractional surface coverage, f, expected from the epitaxial growth conditions. Peak current levels for samples grown at 530 °C and 575 °C are comparable, indicating that the local current flow through the ErAs nanoparticles was similar in these samples. Thus, we set the same threshold current value for samples grown at 530 °C and at 575 °C as a means to assess and compare surface coverage. The images were then divided into 30 nm × 30 nm areas, corresponding approximately to the effective area probed at each point of C-AFM measurement. For each area, the fraction of points with signal levels below the threshold level was computed and taken as a measure of the fractional ErAs coverage within that 30 nm × 30 nm area. This approach provides an estimate of the spatial dependence of the fractional ErAs coverage, as probed by C-AFM. The expected spatial distribution of local ErAs coverage was also modeled numerically for given values of f and nanoparticle radius, r. We assumed that the ErAs nanoparticles nucleated randomly at the pn junction during growth and generated a simulated distribution of ErAs surface coverage by placing nanoparticles of radius r on the surface at random locations until the expected average fractional coverage f was reached. Since the ErAs nanoparticles grown at 530 °C are known to be ~3–4 ML in thickness,[12–14] the corresponding reference surface coverage, f, is about 40% for 1.6 ML of ErAs deposition. As shown in Fig. 1(c) and prior studies,[10] however, ErAs nanoparticle thickness can increase at higher growth temperatures. Simulations of surface coverage were, therefore, performed by placing randomly generated nanoparticles with radii ranging from 4 nm to 10 nm[11,12] and thickness from 4 ML to 16 ML within a 1500 nm × 375 nm area corresponding to the typical area imaged by C-AFM, and at densities corresponding to the known amounts of ErAs deposition for different samples. Figure 4(a) shows simulated ErAs nanoparticle distributions for 6 nm radius and thicknesses of 4 ML, 10 ML, and 16 ML, and total ErAs deposition of 1.6 ML. Each simulated area was then divided into 30 nm × 30 nm blocks and the probability of ErAs coverage in each block was computed for different nanoparticle radii and thicknesses, and compared to statistical distributions of ErAs nanoparticle coverage deduced from experimental measurements. The statistical distributions derived from the C-AFM data correspond most closely to the expected for nanoparticle radius of ~6 nm, and distribution for nanoparticles 6 nm in radius were, therefore, used to estimate the thickness of embedded ErAs nanoparticles.

Figure 4(b) shows the probability distributions of ErAs surface coverage derived from an analysis of C-AFM data for samples with 1.6 ML ErAs grown at 530 °C and 575 °C, along with the simulated distribution expected for 1.6 ML ErAs deposition with ErAs nanoparticle thicknesses of 4

ML, 8 ML, 10 ML, 12 ML, 14 ML, and 16 ML with a fixed nanoparticle radius of 6 nm. Since ErAs deposition was fixed at 1.6 ML, variations in the vertical extent of the ErAs nanoparticles would yield reduced surface coverage, as well as dramatically different statistical distributions of local ErAs surface coverage. For the sample grown at 530 °C, the statistical distribution of surface coverage derived from the C-AFM data agreed well with that expected for 4 ML ErAs nanoparticle thickness, as expected. In contrast, for the sample grown at 575 °C, the distribution derived from C-AFM data agreed with that expected for ~10–12 ML ErAs nanoparticle thickness. Since the coverage distributions were derived from a finite number of simulated particles distributions, there are statistical fluctuations present at low surface coverage, but the overall shape of the distribution is minimally influenced by such fluctuations. It is important to note that the key features in the probability distribution for the samples grown at 575 °C could not be reproduced if the vertical extent of the ErAs nanoparticles was held at a constant 4 ML. These results suggest that at high growth temperature, the ErAs nanoparticles have much greater vertical extent and reduced surface coverage, consistent with the cross-sectional TEM image in Fig. 1(c) and other cross-sectional TEM studies of ErAs for different growth temperature.[10,15] Furthermore, the observation of comparable local current levels for different ErAs nanoparticle thicknesses indicates that ErAs coverage of the junction area is the dominant factor determining the increase in electrical conductivity provided by the nanoparticle layer. Another possible explanation for reduced surface coverage is that some of erbium was desorbing from the surface without vertical extension at the high temperature. However, this explanation seems unlikely, since we observe thicker ErAs particles in TEM images. Therefore, we conclude that the increasing vertical extent of ErAs nanoparticles grown at high temperature and consequent reduction in surface coverage is responsible for the observed reduction in macroscopic tunnel junction conductivity at elevated growth temperature.[6]

In summary, conductive atomic force microscopy was used to characterize electrical conductivity and the associated morphology of ErAs nanoparticles embedded in GaAs pn junctions, prepared via MBE growth. A statistical analysis of C-AFM images for samples grown at different temperatures and ErAs deposition levels indicates that for growth temperatures ~530 °C, ErAs nanoparticles form with a thickness of ~3–4 ML; ErAs nanoparticle interface coverage and the associated electrical conductivity increased linearly with increased ErAs deposition. For growth at 575 °C, the ErAs nanoparticle thickness increased to ~10–12 ML, and the consequent reduction in ErAs interface coverage leads to a corresponding reduction in tunnel junction conductivity. These results explain the dependence of macroscopic tunnel junctions on the growth conditions, provide guidelines and new insight into strategies for optimizing III-V semiconductor tunnel junction conductivity via RE-V nanoparticle incorporation, and highlight the ability of scanned probe metrology combined with statistical analysis of local data on electronic properties to elucidate subsurface electronic and structural behavior at the nanoscale.

Part of this work was supported by the National Science Foundation (DMR-1066430 and CAREER ECCS-0954732), the Judson S. Swearingen Regents Chair in Engineering at the University of Texas at Austin, the Army Research Office (W911NF-11-1-0452 and PECASE W911NF-09-1-0434).

[1]J. M. O. Zide, A. Kleiman-Shwarsctein, N. C. Strandwitz, J. D. Zimmerman, T. Steenblock-Smith, A. C. Gossard, A. Forman, A. Ivanovskaya, and G. D. Stucky, Appl. Phys. Lett. **88**, 162103 (2006).
[2]J. M. O. Zide, D. Vashaee, Z. X. Bian, G. Zeng, J. E. Bowers, A. Shakouri, and A. C. Gossard, Phys. Rev. B. **74**, 205335 (2006).
[3]H. Chen, W. J. Padilla, J. M. O. Zide, S. R. Bank, A. C. Gossard, A. J. Taylor, and R. D. Averitt, Opt. Lett. **32**, 1620 (2007).
[4]C. Kadow, S. B. Fleischer, J. P. Ibbetson, J. E. Bowers, A. C. Gossard, J. W. Dong, and C. J. Palmstrøm, Appl. Phys. Lett. **75**, 3548 (1999).
[5]A. M. Crook, H. P. Nair, and S. R. Bank, Appl. Phys. Lett. **98**, 121108 (2011).
[6]H. P. Nair, A. M. Crook, and S. R. Bank, Appl. Phys. Lett. **96**, 222104 (2010).
[7]J. J. M. Law, E. T. Yu, G. Koblmüller, F. Wu, and J. S. Speck, Appl. Phys. Lett. **96**, 102111 (2010).
[8]P. Tejedor, L. Diez-Merino, I. Beinik, and C. Teichert, Appl. Phys. Lett. **95**, 123103 (2009).
[9]C. Kadow, J. A. Johnson, K. Kolstad, and A. C. Gossard, J. Vac. Sci. Technol. B **21**, 29 (2003).
[10]N. Jourdan, H. Yamaguchi, and Y. Horikoshi, Jpn. J. Appl. Phys., Part 2 **32**, L1784 (1993).
[11]K. W. Park, H. P. Nair, A. M. Crook, S. R. Bank, and E. T. Yu, Appl. Phys. Lett. **99**, 133114 (2011).
[12]B. D. Schultz and C. J. Palmstrøm, Phys. Rev. B **73**, 241407 (2006).
[13]C. Kadow, J. A. Johnson, K. Kolstad, J. P. Ibbetson, and A. C. Gossard, J. Vac. Sci. Technol. B **18**, 2197 (2000).
[14]T. Sands, C. J. Palmstrøm, J. P. Harbison, V. G. Keramidas, N. Tabatabaie, T. L. Cheeks, R. Ramesh, and Y. Silberberg, Mater. Sci. Rep. **5**, 99 (1990).
[15]H. P. Nair, A. M. Crook, D. A. Ferrer, and S. R. Bank (unpublished).